Reaction Mechanism of Adenylyltransferase DrrA from *Legionella pneumophila* Elucidated by Time-Resolved Fourier Transform Infrared Spectroscopy

Konstantin Gavriljuk,[†] Jonas Schartner,[†] Aymelt Itzen,[‡] Roger S. Goody,[§] Klaus Gerwert,*,[†] and Carsten Kötting*,[†]

[†]Department of Biophysics, Ruhr-Universität Bochum, Universitätsstrasse 150, 44801 Bochum, Germany

[‡]Center for Integrated Protein Science Munich (CIPSM), Chemistry Department, Technische Universität München, Lichtenbergstrasse 4, 85747 Garching, Germany

[§]Department of Physical Biochemistry, Max Planck Institute of Molecular Physiology, Otto-Hahn-Strasse 11, 44227 Dortmund, Germany

Ⓢ *Supporting Information*

ABSTRACT: Modulation of the function of small GTPases that regulate vesicular trafficking is a strategy employed by several human pathogens. *Legionella pneumophila* infects lung macrophages and injects a plethora of different proteins into its host cell. Among these is DrrA/SidM, which catalyzes stable adenylylation of Rab1b, a regulator of endoplasmatic reticulum to Golgi trafficking, and thereby alters the function and interactions of this small GTPase. We employed time-resolved FTIR-spectroscopy to monitor the DrrA-catalyzed AMP-transfer to Tyr77 of Rab1b. A transient complex between

DrrA, adenylylated Rab1b, and the pyrophosphate byproduct was resolved, allowing us to analyze the interactions at the active site. Combination of isotopic labeling and site-directed mutagenesis allowed us to derive the catalytic mechanism of DrrA from the FTIR difference spectra. DrrA shares crucial residues in the ATP-binding pocket with similar AMP-transferring enzymes such as glutamine synthetase adenylyltransferase or kanamycin nucleotidyltransferase, but provides the complete active site on a single subunit. We determined that Asp112 of DrrA functions as the catalytic base for deprotonation of Tyr77 of Rab1b to enable nucleophilic attack on the ATP. The study provides detailed understanding of the *Legionella pneumophila* protein DrrA and of AMP-transfer reactions in general.
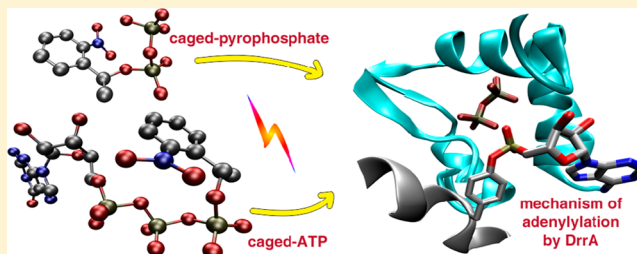
■ INTRODUCTION

Legionella pneumophila is a human pathogen that evades lysosomal degradation by establishing a *Legionella*-containing vacuole (LCV), where the bacterium replicates to high numbers and eventually lyses the host cell.[1,2] A large number of proteins that manipulate diverse host cell functions are injected into the host cell via the Dot/Icm (defect in organelle trafficking/intracellular multiplication) type IV secretion system (TFSS).[3–5] To achieve survival of the pathogen in the LCV, vesicular transport processes of the host cell must be hijacked and manipulated. Small GTPases of the Rab and Arf families play fundamental roles in the regulation of vesicular trafficking and, therefore, present prime targets for pathogenic enzymes.[6,7]

Rab GTPases cycle between the inactive GDP-bound and the active GTP-bound state, and interaction with various effectors only takes place in the latter. Exchange of GDP to GTP is catalyzed by GEFs (guanine nucleotide exchange factors) and hydrolysis of GTP to GDP is catalyzed by GAPs (GTPase activating proteins). Membrane anchoring of Rab GTPases is mediated by C-terminal geranylgeranylation,[8,9] and Rab recycling is mediated by GDI (GDP dissociation inhibitor)

that extracts membrane bound Rab GTPases to form a soluble cytosolic complex.[10] Tight control of Rab function is achieved through this interaction network. The first *Legionella* protein found to directly interfere with Rab function was DrrA (defect in Rab recruitment A), which recruits Rab1b, a regulator of endoplasmatic reticulum to Golgi trafficking, to the LCV.[6,11,12] DrrA consists of three domains: a C-terminal phosphatidylinositol-4-phosphate (PI-4P) binding domain (P4M) mediating membrane localization,[13,14] a central GEF domain for Rab1b,[12,15] and an N-terminal adenylyltransferase (ATase) domain that catalyzes adenylylation of Tyr77 of Rab1b.[16]

Adenylylation involves covalent transfer of an AMP moiety from ATP to a target residue that can regulate the activity of certain proteins.[17,18] In the case of serine, threonine, or tyrosine modification this results in a stable post-translational modification. For Rab1b, adenylylation has only small effects on the GEF activity of DrrA, whereas activation by the GAPs LepB and TBC1D20 as well as interaction with certain

effectors, such as Mical-3, are impaired.[16,19] *Legionella* can reverse these effects by deadenylylation via SidD.[19−21] Thus, the pathogen achieves precise temporal control over the localization and activation state of Rab1b on the LCV through the interplay of DrrA, SidD, and other proteins.

Crystal structures are available for the P4M[14] and GEF[15] domains of DrrA. However, only partial structures of the ATase domain, which do not contain a nucleotide, are available.[16,22] Even if such a structure were available, it would provide a snapshot of the reaction but would lack information about the dynamics of the enzymatic process, which is needed to understand the reaction mechanism. The current view of the adenylylation reaction steps[19] is summarized in Scheme 1.

Scheme 1. General Scheme of the Adenylylation Reaction[a]

$$\text{DrrA} + \text{ATP} + \text{Rab1b} \rightleftharpoons \text{DrrA·ATP·Rab1b} \rightarrow \text{DrrA} + \text{PP}_i + \text{Rab1b-AMP}$$

[a]The educts DrrA, Rab1b, and ATP form the enzyme-substrate complex. Reaction products are adenylylated Rab1b and pyrophosphate (PP_i).

Here, we present an infrared spectroscopical study of DrrA-catalyzed adenylylation of Rab1b using photocleavable caged-ATP and caged-PP_i (pyrophosphate). Fourier transform infrared (FTIR) spectroscopy is a powerful tool for analysis of protein mechanisms at atomic detail in real time.[23,24] We obtained single-turnover kinetic data and identified an accumulating intermediate pyrophosphate-bound state. Site-directed mutagenesis in combination with these data allowed us to identify residues crucial for nucleotide binding and catalysis of AMP transfer.

■ EXPERIMENTAL SECTION

Synthesis of Caged Compounds. npe (P^3-(1-(2-nitrophenyl)-ethyl)-caged nucleotides were synthesized as described elsewhere.[25] α-$^{18}O_2$ and β-$^{18}O_3$ labeled npeATP was synthesized as described elsewhere[26,27] and kindly provided by Dr. Yan Suveyzdis (Department of Biophysics, Ruhr-University Bochum). γ-$^{18}O_3$-labeled ATP was prepared from ADP and $^{18}O_4$-phosphate by means of carbamate kinase[26] and was kindly provided by Dominik Beyer (Department of Biophysics, Ruhr-University Bochum). ^{18}O-labeled phosphate was prepared from PCl_5 (Sigma-Aldrich, Munich, Germany) and $H_2^{18}O$ (99.1 at. % ^{18}O, Campro Scientific, Berlin, Germany). Nucleotides were purchased from Sigma-Aldrich (Munich, Germany). The synthesis scheme for the new compounds npePPi and npe-γ-$^{18}O_3$-ATP is presented in Figure S1 and details are given below.

Synthesis of npePPi. 280 mg of PPi (Sigma-Aldrich, Munich, Germany, in 10 mL water) were mixed with 2.2 g of 1-(2-nitrophenyl)diazoethane (in 6 mL CHCl$_3$) and stirred vigorously in the dark. The pH was adjusted to 3−4 and kept constant by adding 20 μL of 1 M HCl if necessary. Reacted 1-(2-nitrophenyl)diazoethane was removed once a day and a fresh solution was added to the reaction mixture (in total 2.2 g, 733 mg each day). The reaction was monitored by analytical HPLC (reversed phase C18, 50 mM NaPi, pH 6.5, 5 mM *tert*-butylammonium bromide, 15% acetonitrile) and was finished after 72 h. The chloroform phase was removed and the water phase was washed three times with 5 mL of CHCl$_3$. Afterward npePPi was purified over a anion exchange column (DEAE) with a gradient (0−190 mM) of triethylammonium bicarbonate (TEAB) buffer (pH 8). The product fractions were pooled, concentrated, and analyzed by HPLC, ESI-MS, ^{1}H NMR, and ^{31}P NMR. The yield was 225 mg (80.4%). ^{1}H NMR npePP$_i$ triethylammonium salt (400 MHz, D$_2$O, ppm): δ 1.23−1.25 (d, 3H), 1.34−1.37 (t, 18H), 3.25−3.30 (t, 12H), 3.67−3.72 (q, 1H), 6.0 (s, 2H), 7.58−7.62 (t, 1H), 7.84−7.88 (t, 1H), 7.98−8.00 (d, 1H), 8.10−8.12 (d, 1H). ^{31}P NMR npePP$_i$ triethylammonium salt (400 MHz, D$_2$O, ppm): δ −10.86 (s, 2P)

(Figure S2). ESI-MS (negative): npePP$_i$ = 326.03 [M$^−$]. ESI-MS (positive): npePP$_i$ triethylammonium salt =529.93 [M + H$^+$].

Synthesis of npe-γ-$^{18}O_3$-ATP. 50 mg of $^{18}O_3$-ATP (in 5 mL water) were mixed with a large excess of 2 g of 1-(2-nitrophenyl)-diazoethane (in 5 mL CHCl$_3$) and stirred vigorously in the dark. The pH was adjusted to 3−4 and kept constant by adding 20 μL of 1 M HCl if necessary. The reaction was monitored by analytical HPLC and was finished after 24 h. The chloroform phase was removed and the water phase was washed three times with 3 mL of CHCl$_3$. Afterward npe-γ-$^{18}O_3$-ATP was purified over a anion exchange column (DEAE) with a gradient (0−230 mM) of TEAB buffer (pH 8). The product fractions were pooled, concentrated, and analyzed by HPLC, ESI-MS, and ^{31}P NMR. The yield was 12 mg (24%). ^{31}P NMR npe-γ-$^{18}O_3$-ATP triethylammonium salt (400 MHz, D2O, ppm): δ −11.69 (s, 1P), −12.65 (s, 1P), −23.53 (s, 1P) (Figure S2). ESI-MS (negative): npe-γ-$^{18}O_3$-ATP triethylammonium salt =863.31 [M$^−$]. ESI-MS (positive): npe-γ-$^{18}O_3$-ATP = 662.90 [M + H$^+$].

Protein Expression and Purification. Rab1b_3−174 and DrrA_8−533 were expressed in *E. coli* BL21 (DE3) RIL and purified via Ni-NTA- and gel filtration chromatography as described elsewhere.[16,19,24] Rab5a was expressed as a His$_6$-MBP fusion protein (pOPINM vector) in the same manner as Rab1b, and the purification followed the same steps as for Rab1b, except that PreScission protease was used instead of TEV protease. Proteins were stored in 50 mM Hepes pH 7.5, 200 mM NaCl, 2 mM DTT, 2 mM MgCl$_2$, 20 μM GDP.

Preparative Adenylylation. Rab1b_3−174 (2 mg) was incubated with 20 mol % DrrA N451A R453A D480A S483A, 5 mM ATP, and 2 units inorganic pyrophosphatase (Roche, Mannheim, Germany) for 1 h at room temperature and overnight at 8 °C. The protein was subjected to gel filtration in 5 mM Hepes pH 7.5, 5 mM NaCl, 0.5 mM DTT. The procedure is described elsewhere[16] in more detail, the modification here is the addition of inorganic pyrophosphatase.

FTIR Measurements and Data Analysis. For FTIR measurements, Rab1b_3−174 was subjected to buffer exchange to 1 mM Hepes pH 7.5, 2 mM NaCl, 0.05 mM MgCl$_2$, 0.05 mM DTT via a NAP-5 column (GE Life Sciences, Freiburg, Germany). All experiments were performed with Rab1b·GDP rather than Rab1b·GTP, unless specifically stated otherwise. To obtain npeGTP loaded Rab1b, nucleotide exchange was performed as described elsewhere.[24,28]

Since the ATase domain of DrrA is not a soluble construct, DrrA_8−533 was used, which contains the GEF domain of DrrA, and this needed to be inactivated during FTIR measurements. Two strategies were employed to this purpose: use of the DrrA mutant N451A R453A D480A S483A or preparative complex formation with nucleotide-free Rab1b. The mutant protein does not possess GEF activity[15] and does not interfere with the ATase reaction. The complex between nucleotide-free Rab1b and the DrrA GEF domain is of enormous affinity[15] and can thus be generated preparatively with one equivalent of additional Rab1. Both approaches proved equally successful, yielding the same reaction kinetics and difference spectra. The mutant approach is slightly more advantageous because of the lower molar mass of the resulting adenylylation complex, and thus higher protein concentrations can be achieved in the FTIR sample leading to higher signal intensities. The presented kinetics and spectra of adenylylation were recorded with the complexed wild-type DrrA, while the pyrophosphate binding experiments were performed with the mutant DrrA. For complex formation, 3 mg DrrA_8−533 (50 nmol) were incubated with 1.3 mg Rab1b_3−174 (66 nmol) in the presence of 30 μM ZnSO$_4$ and 0.4 units alkaline phosphatase (Roche, Mannheim, Germany) for 4 h at room temperature. The mixture was subjected to gel filtration (16/60 Superdex 75 pg, GE Life Sciences, Freiburg, Germany) in 5 mM Hepes pH 7.5, 5 mM NaCl, 0.1 mM DTT in order to purify the formed complex. The FTIR sample was prepared between two CaF$_2$ windows as described.[29] The final sample composition was 4 mM Rab1b, 4.8 mM DrrA, 20 mM MgCl$_2$, 20 mM DTT, 200 mM Hepes pH 7.5, and 4 mM caged-ATP. The experiments were performed at 293 K and at least 8 individual measurements were averaged to obtain the difference spectra. Photolysis of the caged compounds was performed using an LPX

240 XeCl-excimer laser (308 nm; Lambda Physics/Coherent Laser Systems, Göttingen, Germany) by 40 flashes within 80 ms. A modified Bruker IFS 66v/s or 80v spectrometer in the fast-scan mode was used for the measurement.[30] The data were analyzed between 1800 and 950 cm^{-1} with a global fit method.[31] In this analysis, the absorbance changes ΔA were analyzed with a sum of exponentials with apparent rate constants k_l and amplitudes a_l.

$$\Delta A(\tilde{\nu}, t) = \sum_{l=1}^{n_r} a_l(\tilde{\nu})e^{-k_l t} + a_\infty(\tilde{\nu})$$

For each rate constant, an amplitude spectrum is obtained by global fit analysis. It corresponds to the difference spectrum of the states before and after the reaction in the case of well separated reaction steps, as in this work. In the figures, negative-amplitude spectra $(-a_l(\tilde{\nu}))$ are shown, so that negative bands belong to the disappearing state, positive bands to the appearing state. An amplitude spectrum of the photolysis $a_0(\tilde{\nu})$ is calculated by

$$a_0(\tilde{\nu}) = a_\infty(\tilde{\nu}) - \sum_{l=1}^{n_r} a_l(\tilde{\nu})$$

Structural Alignment. The structural alignment of DrrA (3L0I and 3NKU), GS-AT (3K7D), LinB (3JZ0), and KNTase (1KNY) was performed with the Multiseq[32] plugin of VMD.[33] Due to the overall low structural conservation, the alignment was performed only for the loop containing the conserved catalytically important motif and the adjacent β-strands: DrrA_93–116, GS-AT_682–708, LinB_23–47, and KNTase_31–57 (Figure S3). For DrrA, due to the small overlapping region of fragments 9–218 and 193–550, the relative orientation was modeled via a structural alignment with GS-AT, which has high structural similarity to DrrA, as performed previously.[19] The catalytically relevant residues of GS-AT, LinB, and KNTase are described elsewhere,[34−36] and their position within the aligned structures was used to search for the functionally corresponding residues of DrrA.

■ RESULTS AND DISCUSSION

Single-Turnover Adenylylation Kinetics. Time-resolved FTIR measurements were performed to study the adenylylation reaction, and first-order exponential kinetics were determined. Caged npeATP was flash photolyzed to release ATP before taking the first data point. Thus, adenylylation of Rab1b·GDP by DrrA was triggered and could be described by a monoexponential function (Figure S4). As a control, no reaction was observed after the laser flash in samples containing DrrA and npeATP but no Rab1b (Figure S4). Since a 400-fold higher catalytic efficiency of DrrA toward the active state Rab1b·GppNHp as compared with the inactive Rab1b·GDP was found previously,[19] we also compared adenylylation kinetics of Rab1b·GDP and Rab1b·GTP (Figure 1, A). In order to measure the kinetics with Rab1b·GTP, npeGTP-loaded Rab1b was used instead of Rab1b·GDP and flash photolyzed simultaneously with npeATP to prevent intrinsic GTP-hydrolysis by Rab1 prior to the start of the experiment. We found that the nucleotide state of the GTPase did not influence the adenylylation reaction, since the apparent reaction lifetimes were the same in both cases (16 ± 2 s for the GTP-bound state, 15 ± 2 s for the GDP-bound state at 293 K). However, this does not contradict previous findings because the FTIR experiments were performed at saturating, millimolar protein concentrations. These protein concentrations are considerably higher than the affinities of the DrrA-ATase·Rab1b·GXP complexes, which lie in the micromolar range.[19] Thus, the complex is fully saturated at millimolar protein concentrations and operates at its maximum rate, assuming that complex formation is the rate limiting step in the overall
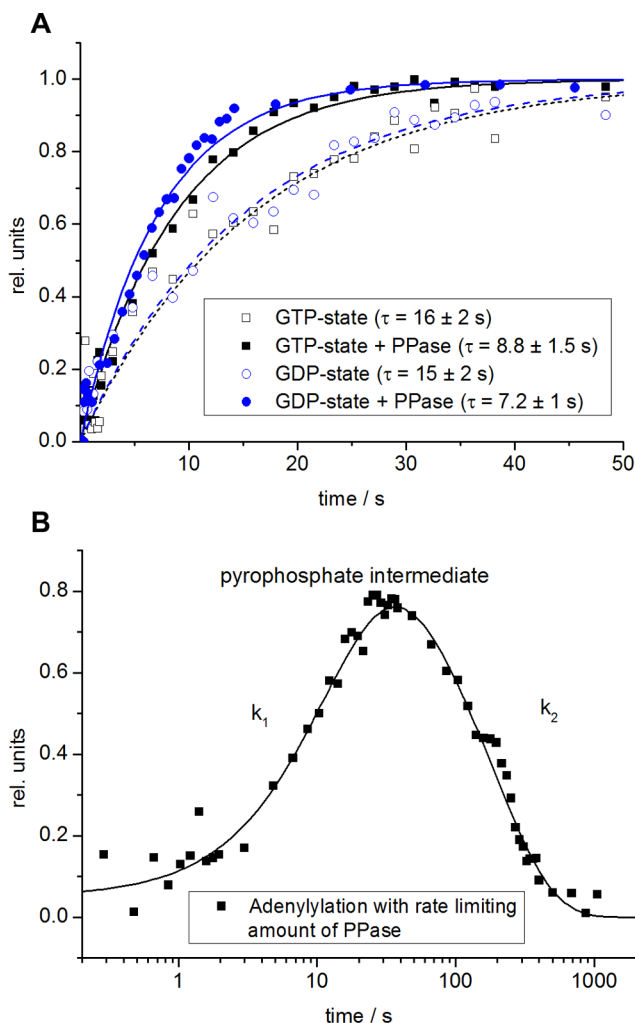

Figure 1. Kinetics of DrrA-catalyzed adenylylation of Rab1b. (A) Normalized time-dependent absorbance changes of the marker bands at 293 K (1089 cm^{-1} for the phosphate of Tyr77-AMP of Rab1b (open data points), and 1078 cm^{-1} for free phosphate (filled data points), respectively without and with pyrophosphatase). Data points for Rab1b in the GDP-bound state are shown as blue circles, for the GTP-bound state as black squares. Solid and dashed lines represent monoexponential fits. While the shown data belong to single representative experiments, the reaction lifetimes are averages from 4−10 independent measurements. Errors are given as standard deviations. (B) Normalized time-dependent absorbance changes showing the appearance of an intermediate in the presence of reaction-limiting amounts of PPase. The accumulating intermediate represents the same state as the end-point of the adenylylation reaction in absence of PPase. We term the observable reaction rates k_1 and k_2, as discussed in the text. The kinetic was derived from a representative band at 1571 cm^{-1} (the actual band is negative in the amplitude spectrum k_1), and the line represents a biexponential fit.

reaction.[16,19] This indicates that only the affinity of DrrA and Rab1b but not the catalytic mechanism differs in the adenylylation reactions of Rab1b·GDP and Rab1b·GTP. A similar situation was found previously for the enzyme stimulated GTP-hydrolysis reaction in the Rap GTPase GAP complex.[37] The switch regions of Rab1b adopt different conformations depending on the nucleotide state, which leads to changes of affinity to DrrA. Additionally, Rab5a, which normally is not a substrate for DrrA,[38] was very slowly adenylylated under FTIR-conditions (131 ± 20 s, Figure S4),

also indicating that affinity-based limitations can be overcome at high protein concentrations under FTIR conditions.

Inorganic pyrophosphate (PP_i) is a byproduct of adenylylation (Scheme 1) and was previously found to slightly inhibit the reaction, an effect that can be avoided by addition of pyrophosphatase (PPase).[19] The use of helper enzymes has also been established in FTIR.[39,40] Here, addition of catalytic amounts of PPase also resulted in acceleration of the reaction, with reaction lifetimes decreasing to 8.8 ± 1.5 s for the GTP-bound state and 7.2 ± 1 s for the GDP-bound state (Figure 1, A). Furthermore, adenylylation and degradation of PP_i can be kinetically separated and fitted biexponentially by using reaction limiting amounts of PPase (Figure 1, B). Thus, apparent reaction rates k_1 (adenylylation + formation of PP_i intermediate) and k_2 (degradation of PP_i intermediate) can be resolved. The PP_i intermediate was then further analyzed with the help of infrared difference spectra of the reaction steps, as will be discussed below.

Amplitude Spectra and Assignment of Phosphate Bands. Global fit analysis yielded not only the reaction lifetimes, but also the corresponding amplitude spectra of the reaction rates and of the photolysis reaction. The spectra allow identifying and understanding the states occurring during the reaction, such as transient protein–ligand complexes. Starting with the photolysis spectrum, we found that npeATP did not bind to DrrA prior to photolysis, and released ATP was also not protein-bound directly after photolysis. This was shown by comparing the phosphate bands in the photolysis spectra of free npeATP (in absence of any proteins) and of npeATP in the DrrA/Rab1b sample (Figure S5). Similar conclusions could be drawn in an earlier FTIR study of the catalytic fragment of the ATP-dependent heavy metal transporter CopB.[27]

Following the photolysis spectrum, the amplitude spectra of the apparent reaction rates k_1 (adenylylation) and k_2 (PP_i hydrolysis) were obtained (Figure 2). As can be deduced from the photolysis spectrum, negative bands in k_1 belong to free Rab1b, DrrA, and ATP. Positive bands belong to the accumulating intermediate state with pyrophosphate and Rab1b-AMP. This state is seen as negative bands in k_2, while positive bands belong to free Rab1b-AMP, DrrA, and phosphate because the intermediate is degraded in k_2. This interpretation was achieved by isotopic labeling of ATP and experiments with caged npePP_i, as will be shown below.

Notably, while the amplitude spectra of k_1 and k_2 have few common bands in the phosphate region, they appear to be mirror images in the amide regions of protein absorption ($1700-1500$ cm^{-1}, Figure 2). This indicates that the intermediate state involves reversible conformational changes of DrrA or Rab1b, or of both proteins. Most of these difference bands cancel each other out in the sum of the amplitude spectra of k_1 and k_2 (Figure 2), and the remaining bands most likely reflect conformational changes of Rab1b that are induced by adenylylation of Tyr77 in the switch II region. Note that the rates k_1 and k_2 can only be separated when reaction limiting amounts of PPase are used. Only one rate with the sum of the amplitude spectra of k_1+k_2 can be resolved with larger amounts of PPase. Without PPase, only k_1 with the corresponding spectrum is resolved as the system becomes arrested in the pyrophosphate-bound state.

α-$^{18}O_2$-labeled ATP was employed in order to assign the bands belonging to the adenylylation process (Figure 3). In the amplitude spectrum of k_1, the α-phosphate vibration of the disappearing ATP at 1258 cm^{-1} and an appearing band at 1089
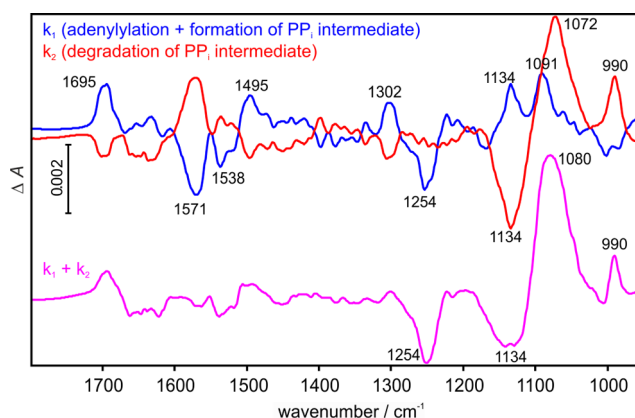

Figure 2. Infrared difference spectra of DrrA-catalyzed adenylylation of Rab1b. In the amplitude spectrum of k_1 (blue), negative bands belong to free Rab1b, DrrA, and ATP, positive bands to the complex of Rab1b-AMP with DrrA and pyrophosphate. In the amplitude spectrum of k_2 (red), negative bands belong to the complex of Rab1b-AMP with DrrA and PP_i, positive bands to free Rab1b-AMP, DrrA, and phosphate. In the sum of the amplitude spectra of k_1 and k_2 (magenta), negative bands belong to free Rab1b, DrrA, and ATP, positive bands to free Rab1b-AMP, DrrA, and phosphate. Adenylylation in absence of PPase yields the same spectrum as that of k_1. The individual rates cannot be resolved when the amount of PPase is not rate-limiting, and the spectrum of k_1+k_2 is obtained in this case.
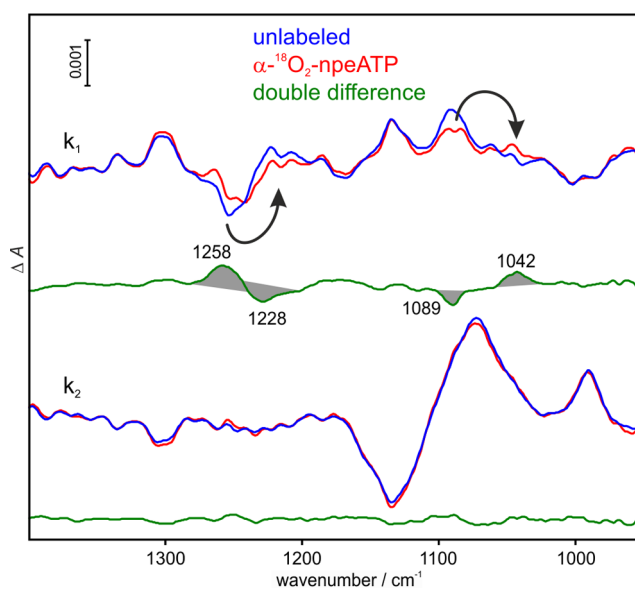

Figure 3. Assignment of the α-phosphate bands in the infrared spectra. Amplitude spectra of the adenylylation reaction steps using unlabeled (blue) and α-$^{18}O_2$-labeled (red) npeATP are compared. In the amplitude spectrum of k_1, negative bands belong to free Rab1b, DrrA, and ATP, positive bands to the complex of Rab1b-AMP with DrrA and pyrophosphate. In the amplitude spectrum of k_2, negative bands belong to the complex of Rab1b-AMP with DrrA and PP_i, positive bands to free Rab1b-AMP, DrrA, and phosphate. The double difference (labeled - unlabeled) is shown in green. The α-phosphate vibration of disappearing ATP is detected at 1258 cm^{-1} in the amplitude spectrum of k_1, while a positive band appears at 1089 cm^{-1} that can be assigned to the phosphate of the adenylylated Tyr77 of Rab1b. In the amplitude spectrum of k_2, no band shifts are observed, indicating that Tyr77-AMP undergoes no changes during degradation of the PP_i intermediate.

cm^{-1} are detected. The negative band at 1258 cm^{-1} is in fact a combination vibration of the α- and β-phosphates of ATP because it also shifts with β-$^{18}O_3$-labeled ATP (Figure S6).

The band at 1089 cm^{-1} can be assigned to the symmetric phosphate vibration of Tyr77-AMP of Rab1b and lies well within the region expected for phosphodiesters.[41] Thus, adenylylation of Tyr77 is shown to occur in the process described by k_1. As expected, no band shifts due to α-phosphate labeling are detected in the spectrum of k_2 as the Tyr77-AMP moiety is not affected by degradation of PP_i by PPase and the conformational changes induced by release of PP_i.

The accumulating intermediate appeared to be a complex of DrrA·PP_i·Rab1b-AMP as judged by reversible conformational changes associated with its appearance and degradation. In order to verify this hypothesis, we performed experiments with npePP_i because dissociation of PP_i from such a complex should be a reversible process. Indeed, we could kinetically resolve binding of PP_i to DrrA and Rab1b-AMP after photolysis of npePP_i. This reverse formation of the PP_i intermediate occurs with an apparent lifetime of 3.2 ± 0.2 s at 293 K and the corresponding amplitude spectrum is mostly the same as that of k_1 (Figure 4). No complex formation was observed in absence of Rab1b, showing that the intermediate state is a ternary DrrA·PP_i·Rab1b-AMP complex (Figure 4). Differences between the spectra of k_1 and the reverse formation of the PP_i intermediate can be attributed to conformational changes of Rab1b due to adenylylation, which are not present in the spectrum of the complex formation with free PP_i (see the spectrum of k_1+k_2 in Figure 2).

Protein-bound PP_i is expected to possess distinct vibrational bands of its phosphates (previously β- and γ-phosphates of ATP) due to specific interactions with the protein. However, assuming a rapid equilibrium with free PP_i, this information would be lost due to random rotation of PP_i. Therefore, we performed experiments with β-$^{18}O_3$ and γ-$^{18}O_3$-labeled npeATP, which both produce identically labeled PP_i. While the observed band shifts differ significantly in k_1 as is expected for β- and γ-labeled ATP, the band shifts in k_2 are the same in both cases (Figures S6 and S7). Disappearing PP_i is detected at 1146/1148 cm^{-1} and phosphate bands appear at 1078 and 990 cm^{-1}. The fact that both isotopic labels produce the same band shifts indicates that the PP_i complex formed in k_1 either in the absence or presence of PPase exists in rapid equilibrium with free PP_i, DrrA, and Rab1b-AMP.

Mutational Analysis of the Catalytic Site of DrrA. In the next step, we identified catalytically relevant residues of DrrA by site-directed mutagenesis. In order to select candidates for mutagenesis we compared the structure of DrrA to the structurally similar DNA polymerase β-like enzymes glutamine synthetase adenylyl transferase (GS-AT), lincosamide adenylyltransferase LinB, and kanamycin nucleotidyltransferase (KNTase). GS-AT adenylylates a tyrosine of glutamine synthetase.[34] LinB is a microbial enzyme that catalyzes adenylylation of the antibiotic clindamycin and thus confers resistance to the drug,[35] while KNTase catalyzes an analogous modification of kanamycin.[36] Since there is no available structure of the complete ATase domain of DrrA, we constructed a structural model of DrrA_9−340 based on structure homology considerations. For this, we performed a structural alignment by MultiSeq[32] of two partial structures of DrrA (3L0I and 3NKU[16,22]) and the structures of GS-AT (3K7D), LinB (3JZ0), and KNTase (1KNY) (Figure S3). Despite the fact that the resulting ATP-binding pocket of DrrA
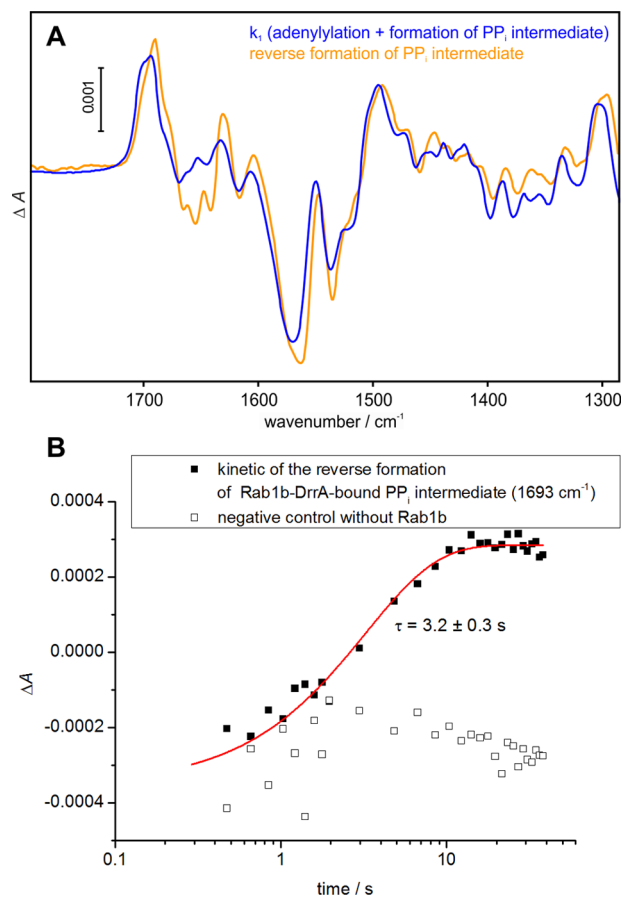

Figure 4. Formation of the PP_i intermediate with help of caged-PP_i. (A) Amplitude spectra of k_1 (blue, same as in Figure 2) and of protein conformational changes following the flash photolysis of npePP_i in the presence of DrrA and Rab1b-AMP (orange) are compared. The spectra are identical for the most part, indicating that the complex of Rab1b-AMP and DrrA with bound PP_i can be formed in the course of the adenylylation as well as by binding of free PP_i to DrrA and Rab1b-AMP. Differences can be attributed to conformational changes of Rab1b due to adenylylation, which are not present in the spectrum of the complex formation with free PP_i (these are expected to correspond to the spectrum of k_1+k_2 in Figure 2). (B) Time-dependent absorbance changes (black squares) of a representative band at 1693 cm^{-1} show the kinetic of the complex formation between DrrA, Rab1b, and PP_i. The reaction can be fitted monoexponentially (red line) yielding an apparent lifetime of 3.2 ± 0.3 s at 293 K. No binding of released PP_i to DrrA in absence of Rab1b was observed (open squares).

is empty and distorted, we were able to localize residues homologous to catalytic side chains of the other enzymes due to the structural similarity.

D110 and D112 of the conserved signature motif G-X_{11}-D-X-D were previously shown to be essential for ATase activity.[16] The structures of GS-AT, LinB, and KNTase in the substrate-bound states revealed a common binding mode for ATP. Generally, a third acidic residue is present, and one of these acidic groups serves as a base for deprotonation of the adenylylated hydroxyl group.[34−36] Furthermore, two positively charged residues and two residues with hydroxyl side chains are required for binding of the triphosphate.[35,36] Notably, not all catalytic residues are provided by the same polypeptide chain in these cases: the active site is complemented by the substrate protein in the case of GS-AT,[34] while it is complemented by a

9342

dx.doi.org/10.1021/ja501496d | *J. Am. Chem. Soc.* 2014, 136, 9338−9345

second identical subunit in the cases of KNTase and LinB, which are homodimeric enzymes.[35,36] Since the binding mode of Rab1b to the ATase domain of DrrA is not known, it could be possible that some of the catalytically acting residues are provided by Rab1b. Therefore, we also mutated residues of Rab1b that are located in the vicinity of the adenylylated Tyr77, but none of these had any impact on the reaction (K46A, R48A, and R79A of Rab1b were tested under FTIR conditions). All analyzed mutants of DrrA are summarized in Table 1. As judged by complete loss of ATase activity, two

Table 1. Mutational Analysis of DrrA[a]

mutant	ATase activity	PP$_i$ binding
D110A	-	-
D112A	-	+
D177A	+	n.d.
S99A	-	n.d.
T106A	-	n.d.
D150A	-	-
K102A	-	n.d.
R158A	+	n.d.
R246A	-	n.d.
D249A	-	-

[a]The table summarizes the impact of mutations of DrrA on the adenylylation activity and on the ability to bind pyrophosphate in complex with Rab1b. "+" indicates wild type-like activity (ca. 90% of WT adenylylation activity for D177A and R158A). "-" means that no adenylylation could be detected during the measurement, indicating at least 100-fold decrease of activity. "n.d." stands for not determined.

positive residues (K102, R246), two polar residues (S99, T106), and four aspartates (D110, D112, D150, D249) were identified as crucial constituents of the active site of DrrA (Table 1 and Figure 5). The location of these residues suggests that a monomer of DrrA is sufficient to form a complete active site, as opposed to LinB and KNTase (Figure 5).

It is of interest that not only three but four acidic residues were found to be important for the reaction. The function of the aspartates is to bind the essential Mg^{2+} ions and to deprotonate the adenylylated group.[35,36,42] The PP$_i$ complex observed during the reaction course allowed us to determine which of the aspartates acts as the catalytic base for deprotonation. For this, we performed the reverse formation of the DrrA·PP$_i$·Rab1b complex with DrrA mutants using npePP$_i$ as above. Only the D112A mutant was able to form the PP$_i$ complex (Table 1). Therefore, it can be concluded that all other identified residues are essential for the binding of PP$_i$·Mg^{2+} or, in general, for the binding of ATP·Mg^{2+}. In contrast, D112 is not required for the interaction with PP$_i$·Mg^{2+} and is probably the catalytic base for the deprotonation of Tyr77 of Rab1b.

■ CONCLUSION

Our single turnover infrared data allow identifying the reaction steps and elucidating the reaction mechanism of DrrA-catalyzed adenylylation of Rab1b. The detailed reaction scheme is presented in Scheme 2. We have shown that npeATP does not bind to DrrA prior to photolysis and thus free DrrA, ATP, and Rab1b are present at the start of the reaction. ATP does not bind to DrrA alone but rather to the complex of DrrA and Rab1b (Figure S5). This step is rate-limiting for the adenylylation, since the DrrA·ATP·Rab1b complex does not
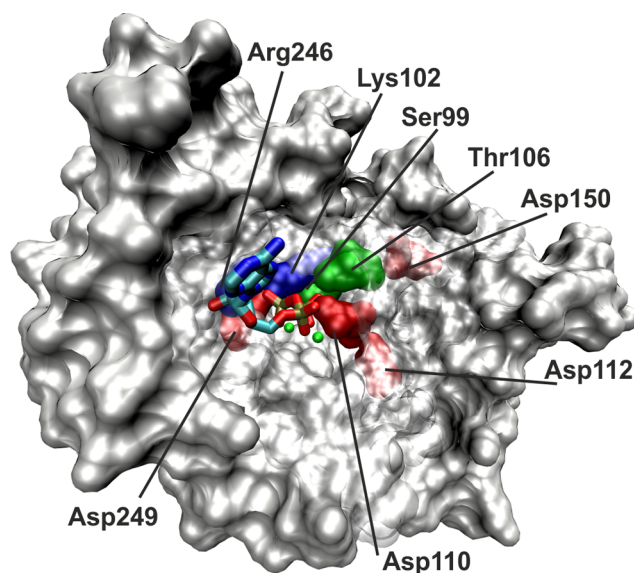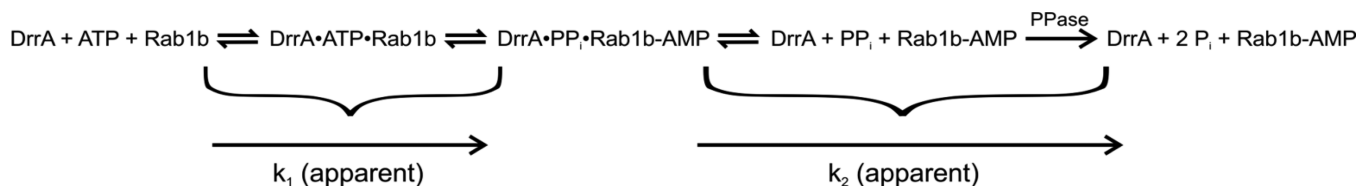

Figure 5. Catalytically relevant residues in the ATP-binding pocket of DrrA. The structural model of DrrA_9−340 is shown in surface representation. The model and the probable position of ATP with Mg^{2+} ions are based on two partial structures of the ATase domain of DrrA (3L0I and 3NKU) that were aligned with the structures of GS-AT (3K7D), kanamycin nucleotidyltransferase (1KNY), and lincosamide adenylyltransferase (3JZ0). Residues that were found to be crucial for ATase activity and form the ATP-binding pocket (see Table 1) are labeled and highlighted (positively charged in blue, negatively charged in red, polar in green). A comparison with the interactions in the ATP-binding site of LinB is shown in Figure S8.

accumulate during the reaction. Possibly, the rate-limiting step is the formation of a binary DrrA·Rab1b complex prior to ATP binding. However, we cannot distinguish between these possibilities. As soon as ATP is bound, Tyr77 of Rab1b is adenylylated and pyrophosphate is created as byproduct of the reaction. These steps proceed with a monoexponential reaction rate k_1 of 0.13 ± 0.1 s^{-1} at 293 K. However, the kinetics rather reflect ATP binding and not the actual adenylylation which occurs at a faster rate that cannot be determined separately. Since pyrophosphate is able to inhibit adenylylation, we expect that the reverse reaction also occurs and have therefore indicated in Scheme 2 that DrrA·ATP·Rab1b and DrrA·PP$_i$·Rab1b-AMP exist in equilibrium.

We could show that the immediate product of AMP transfer is a complex of DrrA, Rab1b-AMP, and pyrophosphate. It exists in dynamic equilibrium with the free components but the complex is thermodynamically favored at the prevailing high protein concentrations in our FTIR experiments. Reverse complex association occurred with an apparent rate constant of 0.31 ± 0.02 s^{-1} (or lifetime of 3.2 ± 0.2 s at 293 K). The dissociation rate of the DrrA·PP$_i$·Rab1b-AMP complex could not be determined but lies obviously between the association rate of the complex and the rate of adenylylation. In the single turnover measurements, dissociation of the pyrophosphate complex and subsequent degradation of pyrophosphate by PPase are described by the apparent reaction rate k_2 (Scheme 2). Degradation of pyrophosphate by PPase is not rate-limiting but can still be kinetically resolved by reducing the amount of PPase.

The molecular reaction mechanism of DrrA was determined by site-directed mutagenesis, while the resolved pyrophosphate intermediate complex proved to be helpful for identifying the

9343

dx.doi.org/10.1021/ja501496d | J. Am. Chem. Soc. 2014, 136, 9338−9345

Scheme 2. Detailed Scheme of the Adenylylation Reaction As Elucidated by FTIR[a]

DrrA + ATP + Rab1b $\rightleftharpoons$ DrrA•ATP•Rab1b $\rightleftharpoons$ DrrA•PP$_i$•Rab1b-AMP $\rightleftharpoons$ DrrA + PP$_i$ + Rab1b-AMP $\xrightarrow{\text{PPase}}$ DrrA + 2 P$_i$ + Rab1b-AMP

k_1 (apparent)　　　　　k_2 (apparent)

[a]While the reaction states can be expected to exist in equilibrium, apparent first-order rate constants are resolved in the FTIR measurements. The complex of DrrA and Rab1b with bound ATP does not accumulate in the reaction and is therefore not observed.

base for deprotonation of the adenylylated tyrosine of Rab1b. Catalytically relevant residues were identified by complete loss of ATase activity in mutated DrrA (Table 1, Figure 5). All identified residues correspond to mechanistically conserved residues of GS-ATase, KNTase, and LinB with the exception that four rather than three acidic residues were found to be important. Therefore, the ATP binding mode can be expected to be very similar to these enzymes.[34−36] Interestingly, all necessary residues of DrrA are located in one polypeptide chain and the active site does not have to be completed by a second enzyme molecule (as in LinB and KNTase) or by the substrate (as in GS-ATase). The binding mode of Rab1b to the ATase domain of DrrA is not known yet, but substrate specificity of DrrA seems not to be dependent on catalytic residues provided by the Rab GTPase. We have shown that the adenylylation rate does not depend on the nucleotide state of the GTPase under millimolar protein concentrations in FTIR measurements. This means that the adenylylation itself is not dependent on the conformational states of Rab1b, which rather govern the overall affinity of the two proteins and thus the catalytic efficiency. Correspondingly, measurements at physiological protein concentrations revealed a clear preference for the GTP-bound state of Rab1b.[19] Probably, both nucleotide states of Rab1b undergo a conformational change upon complex formation with DrrA and ATP, but this state does not accumulate in single-turnover measurements. Furthermore, substrate specificity of DrrA is determined by its affinity to different Rab GTPases but not by any residues of the Rab proteins that would directly contribute to ATP binding or adenylylation. This is demonstrated by the fact that DrrA can adenylylate Rab5a under FTIR conditions while this GTPase is not a substrate for DrrA in vivo.

Notably, not three but four acidic residues were found to be crucial for ATase activity of DrrA (D110, D112, D150, D249). Only D112 was found to be unimportant for the reverse formation of the DrrA·PP$_i$·Rab1b-AMP complex. The suggested reaction mechanism that can be deduced from these findings is depicted in Figure 6. Our data allow us to propose D112 as the base for deprotonation of Tyr77 of Rab1b because it has no function in the interaction with the produced pyrophosphate-magnesium complex. An aspartate acting as a metal ion ligand possesses a lower pK_a than a free aspartate and thus is not able to function as a base for deprotonation.[42] Since D112 does not appear to be involved in magnesium or phosphate coordination, it is suitable for the role of the catalytic base in DrrA. As in KNTase and DNA polymerases,[36,42] two magnesium ions are expected to be present in the active site that are coordinated by three aspartates. D150 appears to be located away from the ATP binding site in the ATP-free crystal structure (Figure 5, 3NKU[16]) but this distortion is probably due to the absence of nucleotide. Therefore, the magnesium ions are most probably coordinated by D110, D150, and D249
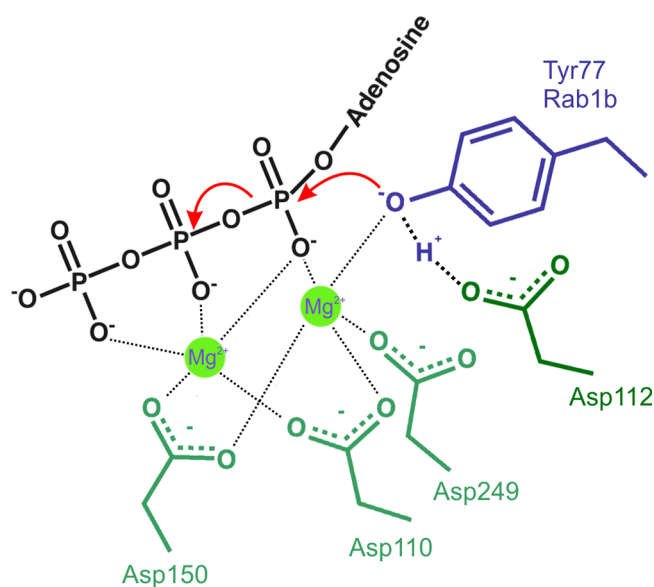

Figure 6. Suggested reaction mechanism of DrrA-catalyzed adenylylation. The Mg^{2+} ions bound to ATP are coordinated by Asp110, 150, and 249 of DrrA (light green), while Asp112 of DrrA (dark green) acts as a base for deprotonation of Tyr77 of Rab1b (blue). Deprotonated Tyr77 nucleophilically attacks the α-phosphate of ATP, and PP$_i$ is released (indicated by the red arrows).

although the exact geometry cannot be deduced from the FTIR measurements.

In this study, we have described the molecular reaction mechanism of DrrA-catalyzed adenylylation of Rab1b. Regulation of protein activity by cycles of post-translational modification, such as adenylylation/deadenylylation or other types of nucleotidylation, is an interesting issue in current research. The importance of the ATase activity of DrrA for retaining of Rab1 on the LCV membrane was recently demonstrated in vivo.[43] L. pneumophila strains carrying the substitutions of D110A and D112A were unable to perform like the corresponding wild-type DrrA and failed to stabilize Rab1 at the LCV membrane. Another example of adenylylation is the modification of Rho GTPases by the Vibrio parahemolyticus effector VopS, which possesses a catalytic FIC domain (filamentation induced by cAMP).[44] The catalytic mechanism of VopS is not known, but could differ from the mechanism of DrrA. It can be expected that new adenylylating enzymes and their targets will be identified in pathological and, possibly, in as yet unknown physiological processes. In proteins which are structurally similar to DrrA, the general features of the adenylylation mechanism should be conserved, but differences may still be found, such as the number of involved acidic residues discussed in this study. Notably, the occurrence of a protein bound pyrophosphate intermediate is reminiscent of

the accumulation of protein bound phosphate prior to its release in the Ras·RasGAP reaction.[26] In that case, the actual bond cleavage occurs in the first kinetic step. In the second step, the electrostatic interactions between the negatively charged phosphate product and positively charged protein residues need to be overcome in order to release the phosphate. Splitting the reaction into two kinetically distinguishable steps leads to lowering of the free activation energy of the overall reaction.[23] This might represent a general feature of phosphoryl transfer reactions. Knowledge of the molecular mechanisms of nucleotidylation might open possibilities for interfering with nucleotidylation-dependent regulation processes, e.g. via pharmacologically relevant inhibitors.

ASSOCIATED CONTENT

Ⓢ Supporting Information

Figure S1, Synthesis scheme of npe-caged PP_i and npe-caged γ-$^{18}O_3$-ATP. Figure S2, ^{31}P NMR of npePP$_i$ and npe-γ-$^{18}O_3$-ATP. Figure S3, Structural alignment of DrrA, GS-AT, KNTase, and LinB. Figure S4, Negative control and reaction kinetics with different GTPases. Figure S5, Photolysis spectra of npeATP in solution and in the presence of DrrA. Figures S6 and S7, Assignment of the β- and γ-phosphate bands in the infrared spectra. Figure S8, Comparison of the ATP interaction pattern in LinB and DrrA. This material is available free of charge via the Internet at http://pubs.acs.org.

AUTHOR INFORMATION

Corresponding Author

carsten.koetting@rub.de; gerwert@bph.rub.de

Notes

The authors declare no competing financial interest.

ACKNOWLEDGMENTS

REFERENCES

(1) Isberg, R. R.; O'Connor, T. J.; Heidtman, M. *Nat. Rev. Microbiol.* **2009**, *7*, 13.

(2) Horwitz, M. A. *J. Exp. Med.* **1983**, *158*, 1319.

(3) Heidtman, M.; Chen, E. J.; Moy, M.-Y.; Isberg, R. R. *Cell. Microbiol.* **2009**, *11*, 230.

(4) Marra, A.; Blander, S. J.; Horwitz, M. A.; Shuman, H. A. *Proc. Natl. Acad. Sci. U.S.A.* **1992**, *89*, 9607.

(5) Berger, K. H.; Merriam, J. J.; Isberg, R. R. *Mol. Microbiol.* **1994**, *14*, 809.

(6) Stenmark, H. *Nat. Rev. Mol. Cell Biol.* **2009**, *10*, 513.

(7) Itzen, A.; Goody, R. S. *Semin. Cell Dev. Biol.* **2011**, *22*, 48.

(8) Casey, P. J.; Seabra, M. C. *J. Biol. Chem.* **1996**, *271*, 5289.

(9) Wu, Y.-W.; Goody, R. S.; Abagyan, R.; Alexandrov, K. *J. Biol. Chem.* **2009**, *284*, 13185.

(10) Alory, C.; Balch, W. E. *Traffic Cph. Den.* **2001**, *2*, 532.

(11) Machner, M. P.; Isberg, R. R. *Science* **2007**, *318*, 974.

(12) Murata, T.; Delprato, A.; Ingmundson, A.; Toomre, D. K.; Lambright, D. G.; Roy, C. R. *Nat. Cell Biol.* **2006**, *8*, 971.

(13) Brombacher, E.; Urwyler, S.; Ragaz, C.; Weber, S. S.; Kami, K.; Overduin, M.; Hilbi, H. *J. Biol. Chem.* **2009**, *284*, 4846.

(14) Schoebel, S.; Blankenfeldt, W.; Goody, R. S.; Itzen, A. *EMBO Rep.* **2010**, *11*, 598.

(15) Schoebel, S.; Oesterlin, L. K.; Blankenfeldt, W.; Goody, R. S.; Itzen, A. *Mol. Cell* **2009**, *36*, 1060.

(16) Müller, M. P.; Peters, H.; Blümer, J.; Blankenfeldt, W.; Goody, R. S.; Itzen, A. *Science* **2010**, *329*, 946.

(17) Itzen, A.; Blankenfeldt, W.; Goody, R. S. *Trends Biochem. Sci.* **2011**, *36*, 221.

(18) Müller, M. P.; Albers, M. F.; Itzen, A.; Hedberg, C. *ChemBioChem.* **2013**, *15*, 19.

(19) Müller, M. P.; Shkumatov, A. V.; Oesterlin, L. K.; Schoebel, S.; Goody, P. R.; Goody, R. S.; Itzen, A. *J. Biol. Chem.* **2012**, *287*, 35036.

(20) Tan, Y.; Luo, Z.-Q. *Nature* **2011**, *475*, 506.

(21) Chen, Y.; Tascón, I.; Neunuebel, M. R.; Pallara, C.; Brady, J.; Kinch, L. N.; Fernández-Recio, J.; Rojas, A. L.; Machner, M. P.; Hierro, A. *PLoS Pathog.* **2013**, *9*, e1003382.

(22) Zhu, Y.; Hu, L.; Zhou, Y.; Yao, Q.; Liu, L.; Shao, F. *Proc. Natl. Acad. Sci. U.S.A.* **2010**, *107*, 4699.

(23) Kötting, C.; Kallenbach, A.; Suveyzdis, Y.; Wittinghofer, A.; Gerwert, K. *Proc. Natl. Acad. Sci. U.S.A.* **2008**, *105*, 6260.

(24) Gavriljuk, K.; Gazdag, E.-M.; Itzen, A.; Kötting, C.; Goody, R. S.; Gerwert, K. *Proc. Natl. Acad. Sci. U.S.A.* **2012**, *109*, 21348.

(25) Walker, J. W.; Reid, G. P.; McCray, J. A.; Trentham, D. R. *J. Am. Chem. Soc.* **1988**, *110*, 7170.

(26) Kötting, C.; Blessenohl, M.; Suveyzdis, Y.; Goody, R. S.; Wittinghofer, A.; Gerwert, K. *Proc. Natl. Acad. Sci. U. S. A.* **2006**, *103*, 13911.

(27) Völlmecke, C.; Kötting, C.; Gerwert, K.; Lübben, M. *FEBS J.* **2009**, *276*, 6172.

(28) John, J.; Sohmen, R.; Feuerstein, J.; Linke, R.; Wittinghofer, A.; Goody, R. S. *Biochemistry (Mosc.)* **1990**, *29*, 6058.

(29) Cepus, V.; Scheidig, A. J.; Goody, R. S.; Gerwert, K. *Biochemistry (Mosc.)* **1998**, *37*, 10263.

(30) Gerwert, K.; Souvignier, G.; Hess, B. *Proc. Natl. Acad. Sci. U.S.A.* **1990**, *87*, 9774.

(31) Hessling, B.; Souvignier, G.; Gerwert, K. *Biophys. J.* **1993**, *65*, 1929.

(32) Roberts, E.; Eargle, J.; Wright, D.; Luthey-Schulten, Z. *BMC Bioinformatics* **2006**, *7*, 382.

(33) Humphrey, W.; Dalke, A.; Schulten, K. *J. Mol. Graph.* **1996**, *14*, 33.

(34) Xu, Y.; Carr, P. D.; Vasudevan, S. G.; Ollis, D. L. *J. Mol. Biol.* **2010**, *396*, 773.

(35) Morar, M.; Bhullar, K.; Hughes, D. W.; Junop, M.; Wright, G. D. *Struct. London Engl. 1993* **2009**, *17*, 1649.

(36) Pedersen, L. C.; Benning, M. M.; Holden, H. M. *Biochemistry (Mosc.)* **1995**, *34*, 13305.

(37) Chakrabarti, P. P.; Daumke, O.; Suveyzdis, Y.; Kötting, C.; Gerwert, K.; Wittinghofer, A. *J. Mol. Biol.* **2007**, *367*, 983.

(38) Müller, M. P. *Mechanisms of reversible enzymatic adenylylation of Rab proteins*; Dortmund University: Dortmund, Germany, 2013.

(39) Eremina, N.; Barth, A. *J. Phys. Chem. B* **2013**, *117*, 14967.

(40) Liu, M.; Karjalainen, E.-L.; Barth, A. *Biophys. J.* **2005**, *88*, 3615.

(41) Guan, Y.; Wurrey, C. J.; Thomas, G. J. *Biophys. J.* **1994**, *66*, 225.

(42) Steitz, T. A.; Smerdon, S. J.; Jäger, J.; Joyce, C. M. *Science* **1994**, *266*, 2022.

(43) Hardiman, C. A.; Roy, C. R. *mBio* **2014**, *5*, e01035.

(44) Yarbrough, M. L.; Orth, K. *Nat. Chem. Biol.* **2009**, *5*, 378.

9345

dx.doi.org/10.1021/ja501496d | *J. Am. Chem. Soc.* 2014, 136, 9338–9345